Particle-In-Cell法を用いた太陽コロナ中の太陽風における プラズマと衛星表面の干渉モデルに関する研究

ガルシア ペレス ホルヘ，鈴木 宏二郎（東京大学）

Plasma-Surface Interaction Modeling Utilizing Particle-In-Cell Code for Solar wind in the Solar Corona Region

Jorge Alberto Garcia Perez, SUZUKI Kojiro (The University of Tokyo, Japan)

ABSTRACT

With the intention of studying the heat up process in the Solar Corona, current scientific efforts involve in-situ measurements with Solar Probes, such as PSP (Parker Solar Probe) mission. In this study, a new Particle-In-Cell code, SCSI (Solar Corona-Satellite Interaction), is developed and tested, with the intention of exploring the phenomena involved in the interaction between the solar wind present in the Solar Corona and the surface of a spacecraft. SCSI is developed with an Object-Oriented approach, allowing features such as several numerical schemes in a single domain, and multigrid meshes. The present program probed successful in replicating the spatial distribution of the species involved and the electric currents present in the system, among other parameters. The floating potential calculated on the probe surface as well as the electric barrier generated around it also show similarities with previous studies on the subject.

1. Introduction

In the area of Solar Physics, one of the biggest mysteries that remains unsolved is to understand the mechanisms through which the Solar Corona, the outermost layer of the Sun before the Heliosphere, can reach up to temperatures that surpass 1 million degrees[1], a phenomenon that conditions the solar wind that engulfs the Solar System and thus affects the Earth.

At the core of this mystery lies the dynamics of the Solar Magnetic field. Current research tries to understand through which mechanisms the energy that is contained in the magnetic lines in the convection zone of the Sun is liberated to the outer layers, and furthermore, how the interaction between the magnetic field and the Solar Plasma that fills the Solar Corona takes place, allowing the particles in plasma state to reach supersonic velocities and the aforementioned high temperatures[1].

In order to solve these questions, currents efforts are directed towards taking in-situ measurements of the parameters of the solar plasma and the magnetic field in the region of the Solar Corona. Missions such as Parker Solar Probe (PSP) and Solar Orbiter (SolO)[1] are currently orbiting the Sun up close and are sending back invaluable information on the characteristics of the Solar Corona.

Under these circumstances, another question arises: which kind of effects can we expect from the interaction between a probe that is immersed in the Solar Corona, and its surrounding environment? Trying to solve this question will allow us both to understand any possible bias in the plasma measurements due to the presence of the spacecraft, and to anticipate any possible hazards that would put these missions at risk.

Table 1 shows the expected environment that the spacecraft PSP will encounter during its closest fly-bys around the Sun (~$8.5R_{\odot}$)[2]. Under these conditions the solar wind is in super-sonic regime. The protons in the plasma, being comparatively heavy, behave almost in ballistic trajectories and thus a wake without protons is formed behind the probe.

Table 1. Reference parameters for this study. In order: density of electrons, protons, electron temperature, proton temperature, solar wind velocity, magnitude of magnetic field, current density of photoelectrons.

Parameter	Value
$n_e = n_p$	7×10^9 m^{-3}
T_e	85 eV
T_p	82 eV
v_{sw}	300 km/s
B_{mag}	2μT
J_{PHE}	16 mA/m^2
Distance to Sun surface	$8.5R_{\odot}$

On the other hand, the electrons respond fast to the changes in the local electromagnetic field and thence are significantly affected by the presence of the probe. Previous research[3] have predicted the formation of a negative floating potential in the surface of the probe, with values around -10 ~ -30 V depending on the dimensions of the probe. This negative value in the potential prevents the fraction of the electron population with the lowest energies to reach the probe, therefore already generating a bias in the temperature and velocity measurements of the plasma.

As for the fraction of electrons that reaches the probe, these electrons interact with the material of the surface and produce the so-called Secondary Emission Electrons (SEE). This new species encompasses new electrons that escape from the atoms of the material thanks to the energy deposited by the impinging electrons, together with the primary electrons that are not absorbed by the surface but still lose some of their energy (non-elastic collision).

The collision of the protons with the surface also generates electrons, but this process is considered insignificant in comparison with the other species in the environment and therefore is generally ignored in analysis[2].

Besides the positive and negative particles in the plasma, and the SEE, yet another new species plays a role in the interaction between the solar wind and the probe: the photoelectrons (PHE) produced in the surfaces of the spacecraft that face the incoming light of the Sun.

Whereas the protons and electrons in the solar wind have high temperatures, PHE and SEE populations are expected to have temperatures less than 10 eV[2], and therefore these two species are highly affected by the local electromagnetic field.

In the present study, a full-PIC simulation is built and tested, with the purpose of investigating the interaction of these four species (protons and electrons from the solar wind, PHE and SEE), the surface of the spacecraft, and the local electric field, under the physical conditions expected at the closest approaches of the PSP mission to the Sun, as listed in Table 1.

2. Simulation Description

The software developed in-house by the authors for this study, called SCSI (Solar Corona – Spacecraft Interaction), is a full-PIC, object-oriented program that aims to simulate the interaction between the Solar Corona plasma and a Spacecraft. However, the code was purposefully created to be highly modular and reusable, with the intention of increasing its application to other plasma-surface interaction set ups.

Since plasma is multi-scale by nature and might involve very different phenomena depending on parameters such as its species composition, the particular characteristics of these species, or external electromagnetic forces, it is convenient in terms of physics or computational performance to use different numerical approaches depending on the particular situation that needs to be analyzed[4].

In order to make a program that can incorporate different numerical approaches without fundamentally changing the code each time, an Object-Oriented-Programming methodology was carried out. Several key factors of a plasma simulation, such as the mesh type, the field solver, or the species treatments at the boundaries, were considered objects that are linked through class attributes and parent-child relationships in tree structures.

Through this approach, the program acquired several functionalities such as the implementation of multigrids or the possibility to host different mesh types and field solvers in a single domain.

The architecture of the program is explained in detail in the next subsection.

2.1 Code Architecture

The program SCSI is entirely written in Python, and it consists of several classes which represent each of the main components of the numerical simulation, a *System* class that contains all these previous classes, a **main.py** file that uses the System object to execute the program, and several auxiliary files.

The separation of the program into classes, and the design of the necessary functions for the code as class functions, help to keep generality as much as much as possible at the moment of writing the code, which translates into increased generality and reusability. Moreover, the use of the concepts of abstract classes and interfaces enforces a clear communication among the different classes, giving robustness and modularity to the code in overall.

As an example of the advantages of this approach, currently the program includes several implementations of electrostatic fields, including constant electric field, time dependent electric field, electric field solved with Successive-Over-Relaxation for the mesh and a Capacity Matrix Method (see 2.3.) for an internal object, among others, and each different mesh inside the domain can have several of these implementations applied to it.

The principal classes of the code are the ones that in total contain all the information necessary for the simulation to execute. These classes are: *System, Boundary, Mesh, PIC, Field, Motion_Solver* and *Species*. At the beginning of the execution, one or several objects of each of the classes are created, and they are stored as attributes of the object derived from *System*. Then, the calling of the functions of these classes is what executes the flow of the code.

Since some of the simulation classes are conceptually different but they are still closely linked in terms of the numerical methods, some classes contain other class instances as attributes, thus facilitating the programming of the class methods. For example, all the Particle-In-Cell functions are contained in the *PIC* class, but since the implementation of these functions depend on the mesh, *Mesh* is stored as an attribute of *PIC*. In the same order of ideas, *Mesh* objects carry one or several *Boundary* objects in a list, and *Field* objects contain a *PIC* object as attribute.

Now, in addition to the connections between classes, the code also hosts connections among objects of the same abstract class for the abstract classes *Mesh*, *PIC* and *Field*.

For two objects of the same abstract class, if one of them acts over a physical region that is contained inside the region of the other object, the two objects are said to have a parent-child relationship, where the child object cannot access the parent object but the parent have full access to the child object. This is translated into the code as a tree structure, where each object can have an arbitrary number of children, and each child in itself can be a parent of other objects.

With this additional relation among objects, an object *Field* which acts on a region 1, for example, has as attribute the *PIC* object that acts on the same region, and it also has as attribute a list of children, which are the *Field* objects acting on the smaller regions inside the region 1.

Since these relationships are dependent on the configuration of the simulation domain, they are particular of each set up. Moreover, each conceptual “region” in the domain needs to have associated its own *Mesh*, *PIC* and *Field* classes. This allows for each region to have a different numerical method, mesh style, etc., and makes the execution flow inside each region similar to a typical plasma simulation with only one mesh.

For a particular class, the added characteristic of having children objects is represented in the code by creating a new class that inherits both the old class and an abstract class that adds the “recursion” feature, forcing the new class to rewrite or add the necessary functions for the

recursion to work.

In practice, all the classes with this feature mostly operate as if they had no children, using the same numerical methods as before; the change is that now some methods are executed before or after the "core" functions in order to deal with the existence of children objects.

As an example of this methodology, let us describe the implementation of the function *computeField* for the class *Electrostatic_2D_rm_sat_cond_recursive,* which inherits from the classes *Electrostatic_2D_rm_sat_cond* and *Field_recursive*.

First, the Field object that acts as the root of the tree executes a modified version of the Capacity Matrix Method from the class *Electrostatic_2D_rm_sat_cond*, where not only the nodes of the underlying mesh but also the nodes of the children meshes in contact with the probe are taken into account. After this, the field in the nodes of the mesh is calculated through a SOR algorithm with Chebyshev Acceleration[4], identically as the case without children. In the next step, the method modifies the values of the field in the nodes of the boundaries of its children fields, through a 2D interpolation of the field values of the parent mesh. Finally, through recursion, the method *computeField* is called for each one of its children.

2.2. PIC

The program SCSI simulates the plasma through the numerical method called Particle-In-Cell (PIC)[4]. In this method, the intention is to model the interactions among particles as close as possible from first principles. In this way, the method is more suitable to study new phenomena, with the drawback of being more computationally expensive.

In PIC, the species present in the plasma are modeled as individual particles that interact with each other. Due to the high number of particles involved in a simulation of this nature, particles are lumped together into "Super-particles" that move with the average velocity of the lumped particles and account for the mass of all of them. As for the interactions, there are two ways of considering the forces present in the system, either by manually summing the interaction of the rest of the particles over each individual particle, or by using Mean-field theory. In the latter, the fields are computed in the nodes of a mesh, and then an interpolation from the node values to the positions of each particle is performed.

In SCSI the second methodology is used, and its computational flow is as follows:

1. From the physical position of particles, particle moments such as density, velocity and temperature are calculated in the nodes of a mesh that overlaps the physical space.
2. The fields are solved from the quantities in the nodes. In the case of SCSI, a finite-difference Poisson solver is used to calculate the electrostatic potential.
3. From the values in the nodes, field values are calculated in the physical positions of each super particle.
4. The particles move forward with a time integrator.

2.3. Numerical schemes

The architecture of SCSI allows to easily switch among different styles of PIC implementations and Poisson solvers; nonetheless, in this section it will be explained the set of numerical schemes that were used for validation of the code, i.e. the simulation shown in sections 3 and 4.

For the time integrator, a Leap-Frog scheme was used. This method is second order accurate in space and time, and it conserves the energy of the system due to its symplectic nature[4].

As for the mesh, a 2D rectangular mesh was used, whereas for the Poisson solver a Successive-Over-Relaxation (SOR) scheme with Chebyshev acceleration was implemented[4].

Both the outer and inner borders of the mesh had a Dirichlet boundary condition, where the outer border of the mesh was kept at 0 V, and the nodes of the inner border, i.e. the surface of the satellite, were computed with the Capacity Matrix Method for conductive surface used in codes such as EMSES[5] and Ptetra[6].

In this approach, at the beginning of the simulation a capacity matrix is calculated for the nodes of the surface of the probe. In this procedure, 1 C of charge is assigned to a node and then the potential generated in the rest of the mesh is solved; the values of the potential for the rest of the nodes on the probe are recorded, and the procedure is repeated over each node of the probe.

Later, while the simulation is executed, the particles that hit the probe are deleted and their charge is stored as accumulated charge at the two closest nodes to the impact location. Then, before the Poisson solver is executed at each step, the accumulated charge and the induced charge generated by the surrounding electric potential are added, and by using the equation $\vec{\phi} = C\vec{q}$ the potential at each node is computed.

The above procedure only accounts for a dielectric surface, where each node can have a different electric potential. Because the satellite is considered conductive the same potential must be established in all the nodes and a redistribution of the accumulated charge is also necessary. This step is carried out by solving the aforementioned capacity equation under the constraint $0 = \sum_i \delta q_i$, being δq_i the change in the charge at node i. This leads to equation 1, ϕ_c being the probe floating potential.

$$\phi_c = \frac{\sum_i q_i}{\sum_i \sum_j C_{ij}} \tag{1}$$

Regarding the PIC interpolation scheme, which connects the values in the physical space to the values in the nodes of the mesh, a linear first-order first-neighbor approach was implemented. If a particle is at a position (x, y) inside the cell denoted by the corners $\{(i,j),(i+1,j),(i,j+1),(i+1,j+1)\}$, the field f in the particle is calculated with equation 2. In the equation, $\mathrm{d}i$ and $\mathrm{d}j$ denote the relative position of the particle within the intervals $\{i, i+1\}$ and $\{j, j+1\}$, respectively. With the opposite process, where the values of the particle are distributed over the neighboring nodes, a similar weighted procedure is used.

$$f(x,y) = f_{i,j}(1-\mathrm{d}i)(1-\mathrm{d}j) + f_{i+1,j}di(1-\mathrm{d}j) + f_{i,j+1}(1-\mathrm{d}i)dj + f_{i+1,j+1}\mathrm{d}i\mathrm{d}j \tag{2}$$

3. Simulation setup

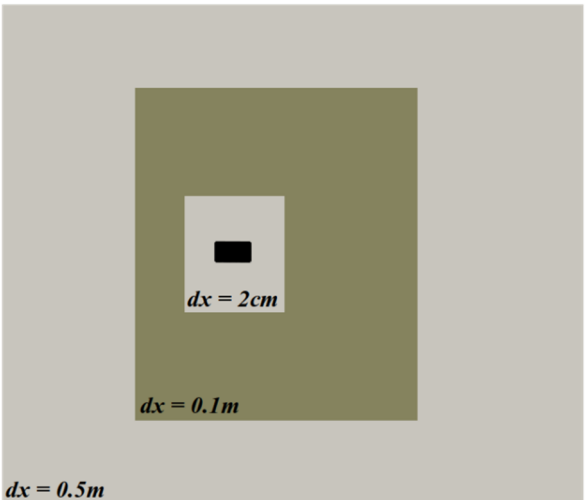

Figure 1. Domain used in the simulation. Each rectangle represents a different mesh, with the distance between nodes as indicated in the image. The probe is the black rectangle situated close to the center of the domain.

The domain used for the results shown in this paper is presented in Fig. 1. The domain is a $W \times H = 35\ \mathrm{m} \times 30\ \mathrm{m}$ rectangular box with a rectangular probe of dimensions $W \times H = 2\ \mathrm{m} \times 1\ \mathrm{m}$. For the calculations of volumetric-related parameters, a depth of 1.0467 m was used in all the domain, with that value chosen to approximate the surface area and light-sided area of the satellite to the values found in the paper by *R. Marchand et al*[2]. The Sun is located in the left side of the domain; therefore, only the left border of the satellite is illuminated (produces photoelectrons), and the Solar wind direction goes from left to right.

In this set up no magnetic field was considered in order to simplify the validation, but this effect is expected to be of minor significance as the gyroradii of the electron populations are in general larger than the dimensions of the satellite[7].

Since the goal is to capture all the possible phenomena that can happen around the spacecraft, in zones where the density of PHE and SEE is predominant a small mesh size is necessary, since the Debye length for SEE and PHE have values around 3cm. On the other hand, in the regions of the domain where the principal source of electrons is that of the solar wind a coarser mesh can be used, as the Debye length for Solar wind electrons is approximately 0.8 m.

For determining the multigrid structure, a first simulation was executed, the Debye length of the three electron species was calculated, and then the mesh configuration was set up accordingly, with the result being what is displayed in Fig. 1. Besides the aforementioned coarse mesh with grid size $\Delta x = \Delta y = 0.5\ m$, two nested mesh were considered, the first one with $\Delta x = \Delta y = 0.1\ m$, and the innermost one with $\Delta x = \Delta y = 0.02\ m$.

The Solar wind in the simulation is modeled as composed by solely protons and electrons, both entering the domain with a Maxwellian distribution according to the parameters shown in Table 1. The particles are loaded into the simulation by creating a thin buffer zone, or "dummy box", around the outer boundary; then, the particles that manage to enter in each time step into the domain are the ones added to the simulation.

The protons, as they hit the spacecraft, are deleted from the simulation and are accounted as charge that accumulates in the surface, while the electrons have a 5% chance of simply reflecting back into the domain without energy loss.

As to the other 95% of the electrons that are absorbed by the spacecraft, they produce Secondary Emission Electrons (SEE) with a yield of 2.9 SEE per incident electron. These new electrons enter the domain from the same location where the incident electrons hit the surface, with random velocity directions that follow in magnitude a Maxwellian distribution of 2 eV of temperature.

As for the photoelectrons (PHE), they are generated uniformly along the left border of the spacecraft, with a rate that produces a flux of 16 mA/m^2. The particles are injected at the surface of the spacecraft, and like the SEE, with random velocity directions and a Maxwellian distribution of 3 eV. The parameters used for SEE and PHE are the same as those found in previous literature on the subject[2], in order to make a more direct comparison of the results and thus validate the code.

4. Results and Discussion

The flow of the SCSI simulation is principally a loop that makes the system advance in time. Thus, the program is kept running and the results are continuously checked, until a stationary state is reached and maintained for some time. Therefore, the results presented here on are temporal averages of the stationary regime of the simulation.

4.1. Potential

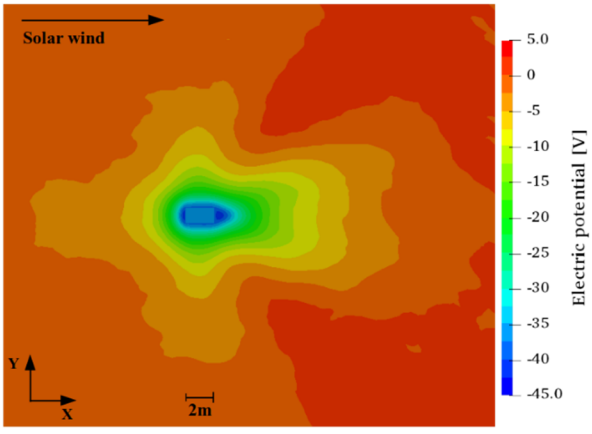

Figure 2. Contour plot of the electric potential. The probe is visible as a blue rectangle in the center, with a potential of -36.4 V.

Fig. 2 shows the distribution of the electric potential in the whole domain. Firstly, it can be observed that the electric potential drop due to the presence of the probe is almost unnoticeable at a distance of ~10 m from it. This indicates that the presence of the spacecraft is damped by the plasma and affects only locally, as expected. The value of the floating potential reached by the spacecraft is -36.4 V, and a region of even lower potential can be observed surrounding its surface. Both phenomena have

been previously described in literature[2,3,7], albeit with different quantitative values.

For example, the potentials achieved by the simulations reported in the paper by *R. Marchand et al*[2] are found in the range -7.6 V to -12.2 V. The reason for this discrepancy might be due to several differences between the set-up of the codes presented in the referenced paper and SCSI. Among those, SCSI considers only a 2D system, whereas the rest of the programs simulated a 3D environment. This implies that the particles simulated with SCSI have only two components of velocity and thus less kinetic energy in comparison with the other simulations. Additionally, although the illuminated and exposed area of the probe in SCSI are almost identical to their counterparts in the aforementioned paper, the geometry of both probes is considerably different.

Now, regarding the region surrounding the probe with lower potential, or potential barrier, this phenomenon can be seen more easily in Fig. 3 and 4, where 1D profiles of the potential are displayed.

Fig. 3 shows a section of a horizontal cut of the mesh that goes through the center of the satellite, as well two of the results found in the paper of *R. Marchand et al*[2], where for ease of comparison the dimensions of that satellite were scaled to match the front and rear parts of the spacecraft modeled in SCSI.

The profile of the potential in all cases exhibits a constant floating potential in the region occupied by the satellite and a steep potential barrier both in the ram and wake regions.

As for the ram section, this phenomenon occurs due to the high concentration of electrons that are created in the front side, counting both PHE and SEE populations. In this region, the density of both populations exceeds that of the free stream Solar wind, and because of this, a net negative potential with respect of the satellite floating potential is generated. As expected, the plasma gets to screen this local effect around a couple of Debye lengths away from the barrier location. In this case, the predominant electron populations are PHE and SEE, meaning a value of $\lambda_D \approx$ 3 cm, which goes in agreement with the position of the barrier around 12 cm away from the surface of the probe.

In the wake, however, a different analysis is necessary. In the rear part of the spacecraft a SEE population is also generated, but its density is not enough to generate a potential barrier as deep and wide. In this case, there is an absence of Solar wind protons due to the probe presence in the fluid. The unbalance of charges generated in the region is what creates the potential well, and as it can be seen in Fig. 5.a), the plasma potential starts to stabilize itself as soon as the proton population appears again.

On the other hand, Fig. 4 displays the electric potential for a 1D vertical cut that traverses the center of the satellite, thus showing the potential barrier generated at the sides of the probe. These potential barriers at each side of the spacecraft are almost identical and have a value of -1.4 V. In this case, the only species that contributes to the formation of the barrier is the Secondary emission electrons, which explains why the barrier at the sides have less amplitude than the ram and wake barriers.

It is interesting to notice how, despite the discrepancy of values in the floating potential between SCSI and the two references from literature, the profiles of the three simulations are reasonably similar. This suggests that the main physical processes are simulated in SCSI to a good

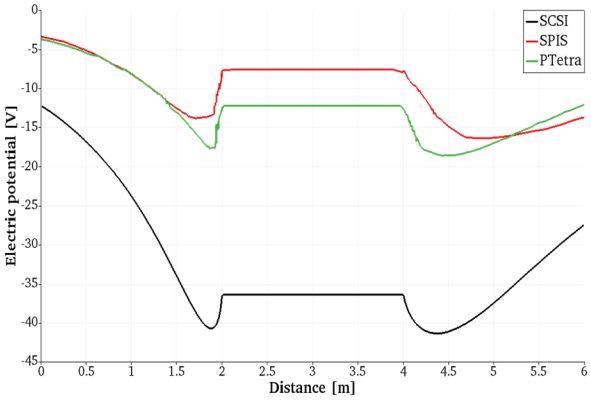

Figure 3. Zoom up of a 1D horizontal cut of the Electric potential, going through the center of the probe. The image shows the result of the potential as well as the results from the softwares SPIS and PTetra extracted from *R. Marchand et al*[2]. The reference potentials are rescaled to match the size of the SCSI probe.

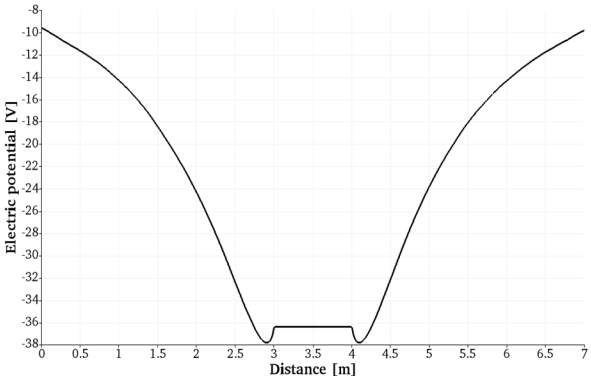

Figure 4. Electric potential for a zoom up of a 1D vertical cut through the center of the probe.

extent, and that the difference in the potential result is considerably dependent on some minor effects. This will be explored in more detail in the next subsection.

4.2. Currents

The electric currents established at the stationary state are a major indicator on how the equilibrium was achieved. This is because the stationary state is reached when the net current into and from spacecraft equals 0. Furthermore, the system behaves as a physical system reaching a minimum of energy: if the potential is more negative, the spacecraft attracts more positive charges and less negative charges, making the incoming current positive and thus charging the surface with more positive charges, which in turn generate a more positive potential. The same process happens if the potential is more positive than expected. Thus, a balance among the incoming protons and electrons from the Solar wind, and the emitted and recollected PHE and SEE populations has to be achieved in order to get a stable potential.

Table 2 shows a comparison between SCSI and SPIS results[2] for the incoming and outgoing currents for all the species, the recollection rate for PHE and SEE species, and the important parameters of the electric potential.

As observed, all the parameters related with the currents

are similar between the two simulations, with the biggest difference being the proton incoming current with a difference in value of 13%. This suggests that although the system is very stable and seems to always reach a stationary floating potential value, the value in itself is highly dependent on the parameters of the system; for example, the physical properties of the surface, the spacecrafts' geometry, or the exposed area to the sunlight.

Table 2. Comparison of the results in current, SEE and PHE recollections, and potential parameters, for the codes SPIS[2)] and SCSI.

Parameter	SPIS	SCSI
I_p (in) [mA]	0.62	0.54
I_e (in) [mA]	-8.4	-7.03
I_{SEE} (out) [mA]	21.2	20.4
I_{SEE} (in) [mA]	-16.2	-15.72
I_{PHE} (out) [mA]	16	16.76
I_{PHE} (in) [mA]	-13.3	-14.38
SEE in/out [%]	76.4	77.61
PHE in/out [%]	83.12	85.83
Satellite Pot. [V]	-7.6	-35.5
Ram pot. [V]	-5~-6	-4.3
Wake pot. [V]	-10	-5.1

It is also worth to notice the small effect that the variation of the probe potential had in the fraction of Solar wind electrons that reach the surface. This is because, for the distribution function of Solar wind electrons, which in literature is usually assumed to be Maxwellian[2)], cutting off the fraction of the population with less than a certain energy produces similar results in the range 10-30 eV.

Additionally, it is also important to mention that the PHE and SEE populations are largely regulated by the potential barrier, which in itself is mostly regulated by the density of these two species. These two effects mentioned above, together with the fact that the protons are negligibly affected by the potential, is what makes the final floating potential so easy to vary without affecting the whole equilibrium of the system.

4.3. Species densities

Fig. 5 shows a series of density distributions for the 4 species included in this simulation. In order, from top to bottom: a) Protons, b) Solar wind electrons, c) Photoelectrons, and d) Secondary emission electrons. For protons and electrons, the parameter plotted is the local density over the free stream density ($n_0 = 7 \times 10^9$ m^{-3}), whereas for PHE and SEE populations the local density was divided over the maximum density found in the mesh. These values are, respectively, 1.1×10^{11} m^{-3} and 3.0×10^{10} m^{-3}. The images presented are close-ups to the vicinity of the probe.

The protons, as mentioned in the introduction, behave almost ballistically. The temperature of this species (82 eV) implies a velocity distribution with mean speed of 1.35×10^5 m/s that is added in random directions to the population, which already has a velocity of 3×10^5 m/s in the $+x$ direction due to the Solar wind. Moreover, owing to their comparatively high mass, the protons are almost negligibly affected by the potential distribution around the spacecraft. Because of this and the fact that the bulk velocity component is higher than the temperature velocity component, this population simply creates a wake behind the spacecraft as it can be seen in the image, and the nominal value of free stream density is reached already around 10 m downstream.

The absence of protons that is observed right behind the spacecraft is what creates the local unbalance of charge in the plasma and therefore the potential barrier present in the wake region.

In the case of electrons, it is more visible the effect of the negative potential in its spatial distribution. Since electrons are lighter than protons and thus more susceptible to the electric field, and their temperature component of the velocity (6.70×10^6 m/s) is around 20 times bigger than the Solar wind component, the satellite basically behaves as an electrode set at a negative potential that repels the fraction of the population with insufficient energy. Actually, according to the Boltzmann model, for an electron temperature of 85 eV and a floating potential of $\phi_{sc} = -36.4$ V, only $\exp(e\phi_{sc}/k_B T_e) \sim 0.65$ of the population will be able to reach the probe, which is in agreement to what is found in the Fig. 5.b).

Another aspect of the plasma behavior that can be verified in Fig. 5.b) is the screening of the probe potential after a couple of Debye lengths. In the $-y/+y$ sides of the spacecraft, we can observe this phenomenon happening at 3-4 meters away from the spacecraft surface, which is around 4-5 Debye lengths for the Solar wind. This effect is less clear in the front and rear sides of the spacecraft because in these regions other phenomena are involved.

Fig. 5.c) shows the density distribution for the photoelectron species. As expected, most of the particles are concentrated in the front side of the probe, and due to the presence of the potential barrier, a significant fraction of the generated particles ends up being recollected by the surface and thus the PHE population depletes quickly as we move further from the surface. Indeed, the potential barrier is located around 12 cm away from the surface, and at 20 cm, the PHE density is approximately 4% of the maximum density.

It is also interesting to notice how the PHE population extends to the sides of the probe. The reason for this effect is that although the photoelectrons injected at the surface of the probe have no negative values in the x component of the velocity, the potential barrier generated at the front reflects back the particles, and, in general, most of them end up being recollected by the probe. However, a portion of the PHE population has sufficient velocity in the component along the surface and the particles manage to escape the probe by crossing the barrier at the sides, which is significantly lower in value.

A similar effect can be observed in the distribution of the SEE species, displayed in Fig. 5.d). Since the electrons from the Solar wind are almost unaffected by the differences in the potential barrier between the front, rear, and side regions of the probe, it is reasonable to assume that all surfaces of the spacecraft receive similar amounts of electron flux; this, in turn, implies that a similar rate of SEE particles are created at all sides of the probe.

Consequently, the concentration of the SEE population at the sides of the probe obeys to the lower potential barrier that these particles need in order to cross in these regions.

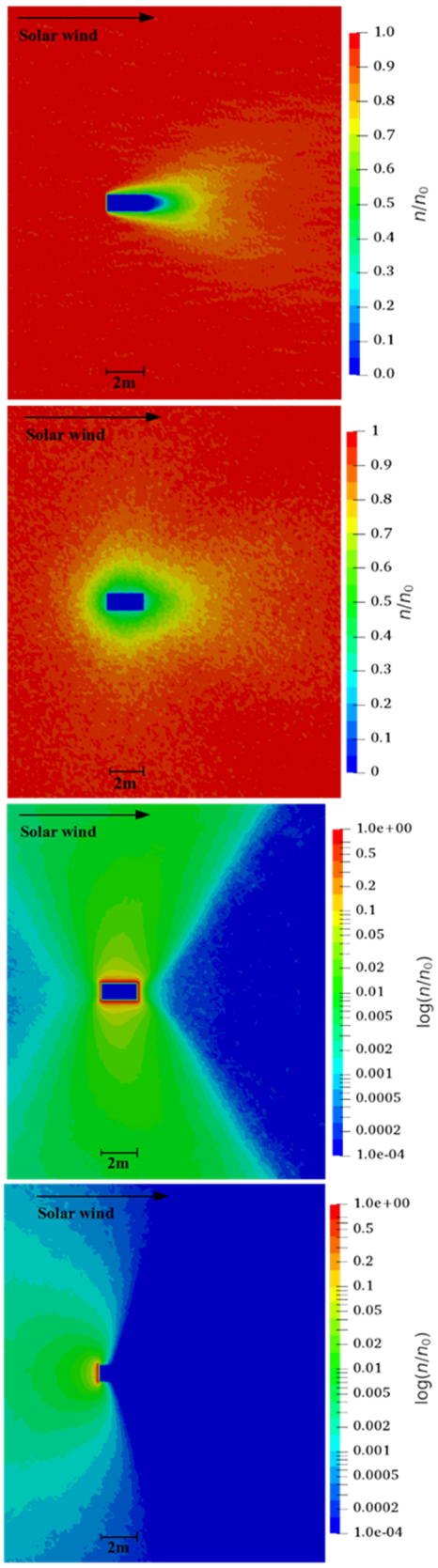

Figure 5. Close-ups of the relative density distribution of species. From top to bottom: a) protons, b) electrons, c) photoelectrons, d) secondary emission electrons.

Moreover, although the ram and wake potential barriers are similar in magnitude, the fact that the wake potential barrier extends in a greater area causes that almost no SEE population can be found in the rear side of the probe, as opposed to the front side, where the potential barrier is mostly one-dimensional.

4.4. Cylindrical mesh set up

As mentioned in section 4.1., a possibility for the discrepancy between the satellite potential found in SCSI and previous codes might lie on the use of a 2D mesh instead of a 3D one. In particular, considering the velocity of the particles in 2D reduces the amount of kinetic energy that they contain. In order to check the impact of this effect in the results, another simulation was performed where only the velocity was considered in a 3D fashion.

The domain was a $W \times H = 22\ \mathrm{m} \times 10\ \mathrm{m}$ rectangular box with a rectangular probe of dimensions $W \times H = 1.2\ \mathrm{m} \times 0.6\ \mathrm{m}$. However, the mesh represents a system with cylindrical symmetry with the axis on the bottom border, thus transforming the actual shape of the probe to a cylinder.

For the time integrator, a modified Leapfrog scheme was implemented which could work in the 2D-3D approach mentioned above. The velocities of the particles were considered in three dimensions: (z, r, ϕ), and the positions in two dimensions: (z, r). At the moment of advancing the particle, as in a typical Leapfrog scheme, the velocity is modified depending on the forces acting in the particle. Despite the velocity having three components, since the mesh is considered cylindrically symmetric, there is no force acting in the $\hat{\phi}$ component, and thus only the $(\hat{z}, \hat{r})$ components are modified.

After the velocity update, the position is further updated by being temporarily considered in three dimensions. Let us call the position in the previous step $\vec{r}_0 = (r_z, r_r)$, the new velocity at the half-step $\vec{v}_{1/2} = (v_z, v_r, v_\phi)$, and the time step Δt. It is important to recall that the component v_ϕ of the velocity is in Cartesian coordinates, rather than angular coordinates, and therefore its units are $\mathrm{m/s}$. With this, the temporary 3D position will take the form $\vec{r^*} = \left(r_z + v_z \Delta t, r_r + v_r \Delta t, v_\phi \Delta t\right) = (r_z^*, r_r^*, r_\phi^*)$. Because the mesh actually stores the information of the (z, r) components instead of the components of a Cartesian coordinate system, a transformation between these two systems is necessary, being performed as $\vec{r}_1 = (r_z^*, \sqrt{r_r^{*2} + r_\phi^{*2}}, 0)$. In this manner, the particle is moved back to the plane (z, r) depicted by the 2D mesh and this $\vec{r}_1$ position is the one stored in the simulation.

In a similar way, the velocity $\vec{v}_{1/2}$ is rotated by an angle $\theta = \tan^{-1}\left(r_\phi^* / r_r^*\right)$ such that v_z, v_r are contained in the (z, r) plane and v_ϕ is perpendicular to the plane. This rotated version of the velocity is the one stored in the simulation.

This modified Leapfrog method, since it still acts in time as a normal Leapfrog scheme, keeps the second order accuracy in space and time, and it conserves the energy of the system.

The results with the new simulation are shown in Fig. 6, making a comparison with the previous results presented in Fig. 2. In this case, the satellite potential reached a value of -15.4 V, suggesting that the consideration of the velocity of

the particles in 2D was the major issue for the difference in potential with the previous set up.

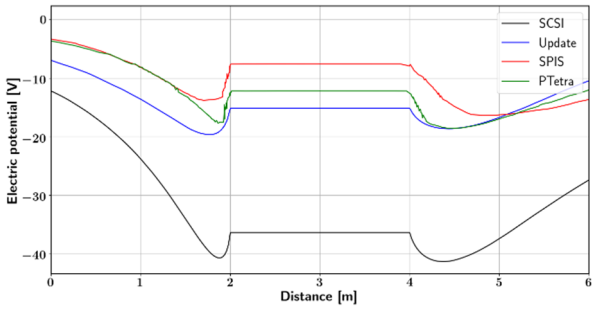

Figure 6. 1D horizontal cut of the Electric potential, going through the center of the probe. The image shows the previous results in Fig. 3, in addition to the potential achieved with the 2D cylindrical mesh simulation, indicated as "Update".

4.5. Summary of SCSI code

A new PIC-based program called Solar Corona – Satellite Interaction (SCSI) has been built, with the intention of studying the physical processes that govern the interaction between the surface of a satellite and the solar wind in the region of the Solar Corona. The code has been developed with an Object-Oriented-Programming approach, in order to make it adaptable to different numerical schemes in Plasma Physics and thus expand its usage to include new physical phenomena and model other problems of interest that involve plasma-surface interactions.

As a benchmark problem to validate SCSI, we have modeled the scenario of a probe immersed in the Solar Corona region at a distance of 8.5 $R_{\odot}$ from the surface of the Sun, inspired in the circumstances that PSP will encounter in its closest approaches to the Sun.

The results of SCSI have been mostly compared to the modeling setup described in the paper by *R. Marchand et al*[2]. The SCSI simulation showed good agreement with the literature in relation with the important parameters of the system, including the probe surface potential, the density distribution of the species included (protons and electrons from the solar wind, photoelectrons and secondary emission electrons), as well as the currents established in the stationary regime.

However, there was a small discrepancy in the value of the floating potential reached in the stationary state, with the SCSI value being -15.4 V and the values achieved by the softwares in *R. Marchand et al*[2] in the range -7.6 V ~ -12.2 V. This difference may be attributed to dissimilarities in the geometry of the probes in both studies, as well as the fact that the SCSI code simulated the scenario in a cylindrically symmetric 2D mesh, as opposed to the 3D fashion used in *R. Marchand et al*. softwares.

5. Conclusions

The appearance of this discrepancy in the surface potential, in contrast with the similarities in the rest of the physical parameters, suggests a high dependence of the final value of the potential on the parameters of the physical situation, such as the probe's geometry or the type of surface material. However, SCSI proved to be capable of reproducing the main physical processes in this scenario up to current standards.

The variance in the surface potential, as well as the changes in the spatial distribution of density for the particles in the solar wind, suggests: 1. There is room for improvement in the field area of surface potential calculation, as currently many of the simulators still differ in their results[2], and the final value of the potential may affect the performance of the missions. 2. The existence of a floating potential as well as PHE and SEE populations may hamper the accuracy of instrument measurements; as such, these phenomena have to be taken into account when considering new space missions with the Sun as their target.

6. Future work

Current efforts are being made on including the interaction of neutral species generated by the ablation of the heat shield with the already present particles. The ionization of these neutral species may also play a role in the precision of the instruments on board, and thus it becomes relevant to study this phenomenon in more detail.

References

(1) Viall, Nicholeen M., and Joseph E. Borovsky, Nine outstanding questions of solar wind physics, Journal of Geophysical Research: Space Physics, 125.7, 2020, p. e2018JA026005.
(2) Marchand, Richard, et al, Cross-comparison of spacecraft-environment interaction model predictions applied to solar probe plus near perihelion, Physics of Plasmas, 21.6, 2014, p. 062901.
(3) Ergun, R. E., et al, Spacecraft charging and ion wake formation in the near-Sun environment, Physics of Plasmas, 17.7, 2010, p. 072903.
(4) Hockney, Roger W., and James W. Eastwood, Computer simulation using particles, crc Press, 2021. p. 20, 195.
(5) Miyake, Yohei, and Hideyuki Usui, New electromagnetic particle simulation code for the analysis of spacecraft-plasma interactions, Physics of Plasmas, 16.6, 2009, p. 062904.
(6) Marchand, Richard, PTetra, a tool to simulate low orbit satellite–plasma interaction, IEEE Transactions on Plasma Science, 40.2, 2011, p. 217-229.
(7) Guillemant, Stanislas, et al, Simulation study of spacecraft electrostatic sheath changes with the heliocentric distances from 0.044 to 1 AU, IEEE Transactions on Plasma Science, 41.12, 2013, p. 3338-3348.